Grain size dependency in sandbank modeling for the case of uniform sediment

Déborah Idier, H.H. van Der Veen, S. Hulscher

JOURNAL OF GEOPHYSICAL RESEARCH, VOL. 114, F03021, doi:10.1029/2008JF001140, 2009

Grain size dependency in sandbank modeling for the case of uniform sediment

D. Idier,[1] H. H. van der Veen,[2] and S. J. M. H. Hulscher[2]

Received 25 August 2008; revised 19 May 2009; accepted 19 June 2009; published 30 September 2009.

[1] A 2-D depth-integrated stability analysis designed for marine tidal sandbanks is developed to investigate the relative influence of the grain size–dependent parameters on the simulated dynamics of the sandbanks for the case of uniform sediment. The model is applied to a real case in the North Sea. Assuming that the model is valid mainly in an area where bed load is the dominant sediment transport mode, the model taking into account the grain size dependencies gives a better prediction of sandbank occurrence than models neglecting these dependencies. All the grain size–dependent parameters are investigated separately. Focusing on the morphological time and wavelength of the sandbanks, this paper demonstrates that neglecting the grain size dependencies, especially the transport threshold, has a drastic influence on the dynamics of modeled sandbanks, especially on the sandbanks growth rate. The influence on the geometrical properties (wavelength and orientation) is less pronounced.

Citation: Idier, D., H. H. van der Veen, and S. J. M. H. Hulscher (2009), Grain size dependency in sandbank modeling for the case of uniform sediment, *J. Geophys. Res.*, *114*, F03021, doi:10.1029/2008JF001140.

1. Introduction

[2] The southern North Sea is covered by sandbanks having typical wavelengths of several kilometers up to 10 km (Figure 1), a height up to tens of meters and an oblique, counterclockwise, orientation with respect to the tidal currents [*Stride*, 1982]. Moreover there is a homogeneous spacing in the sandbank groups. Some other types of bed forms are also found in the North Sea, including shoreface-connected ridges, which have a clockwise crest orientation with respect to the currents, and sand waves, which have smaller height and wavelength and are oriented more or less perpendicular to the dominant current. These rhythmic bed forms occur in a variety of shallow shelf seas and are of interest regarding their role in the protection of the coast and as source of sand. Sandbanks can also be a danger for navigation. Therefore, there is a need to better understand their behavior.

[3] Sandbank generation was initially studied by *Huthnance* [1982]. Using a linear stability analysis and taking into account bed load transport of uniform sediment, he reproduced rhythmic bed forms having the same wavelength and orientation. Even though the shape of real sandbanks is quite complex, it is commonly observed that they have typical spacing and orientation (Figure 1). Grain size dependency has not been investigated in this model yet, however some parameters are grain-dependent. Considering hydrodynamic and sediment mass conservation equations, we can identify four main parameters depending on the grain size: the friction coefficient, the sedimentary coefficient (related to the chosen bed load formula), the critical velocity, U_c, above which sediment is transported and the so-called bed slope coefficient (which is equal to the cotangent of the sediment repose angle).

[4] Heretofore, sandbank generation has mainly been studied using stability analysis based on unimodal sediment and neglecting the sediment transport threshold [*Huthnance*, 1982; *Hulscher et al.*, 1993]. In *de Swart and Hulscher* [1995], a fixed sediment threshold was taken into account in a unimodal two-dimensional depth-integrated (2DH) stability analysis. Recently, *Besio et al.* [2006] performed a 3-D stability analysis to investigate the formation of sand waves and sandbanks. However, in none of these studies was the influence of the grain size dependency of the critical velocity or of the other grain size–dependent parameters investigated.

[5] In the present paper, we study the grain size dependency of sandbank dynamics, for unimodal sediment, focusing on the four parameters identified above. For this purpose, we first develop a 2DH linear stability model for a flat bed subject to a tidal current. Second, in order to estimate if this model gives improved sandbank occurrence prediction, it is applied to North Sea configurations and the results are compared to field observations. In section 4, the sensitivity of the model to the grain size–dependent parameters is investigated and discussed.

2. Model

2.1. Phenomena Taken Into Account

[6] Prior studies have been based on the linear stability approach, either with a 2DH model [*Hulscher et al.*, 1993; *Idier and Astruc*, 2003], or with a 3-D model [*Besio et al.*,

[1]BRGM, Orléans, France.
[2]Water Engineering and Management, University of Twente, Enschede, Netherlands.

0148-0227/09/2008JF001140$09.00

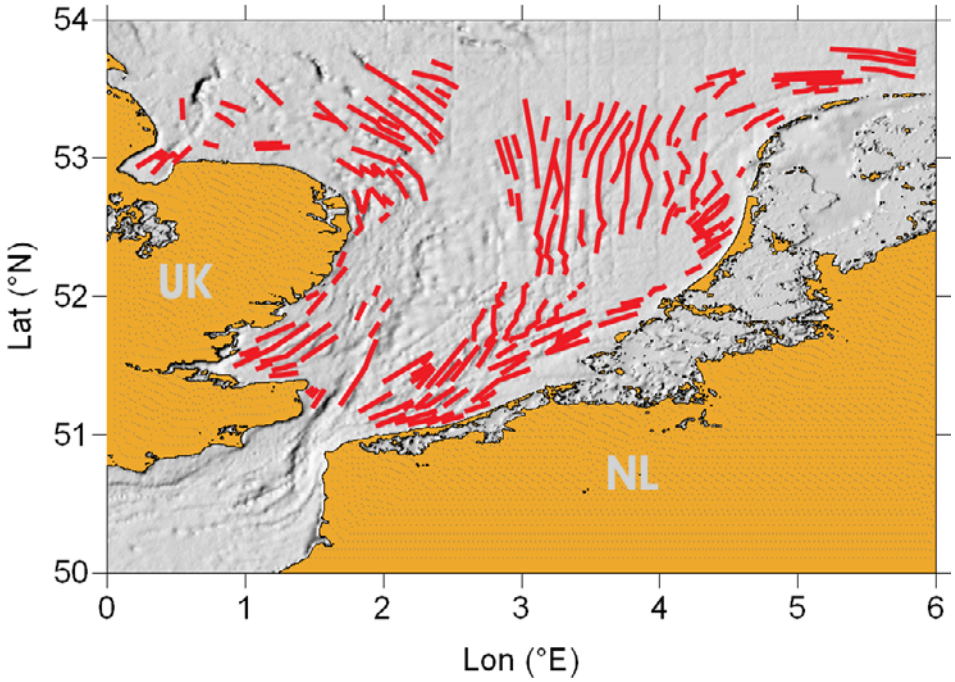

Figure 1. An overview of the southern part of the North Sea. The red lines show the locations of sandbanks [*Van der Veen*, 2008]. Bathymetric data: SRTM30-PLUS V5.0 September 2005 [*Smith and Sandwell*, 1997].

2006]. In addition to the tidal currents, bed load and bed slope transport considered by *Huthnance* [1982], some models have been developed to take into account suspended sediment [*Walgreen et al.*, 2002, 2004], the wave effects [*Roos*, 2004], and even sediment mixtures [*Roos et al.*, 2007].

[7] *Walgreen et al.* [2002] investigated the growth of large-scale bed forms due to storm-driven and tidal currents. They showed that shoreface-connected ridges are mainly formed during storm conditions, whereas the more offshore located tidal sandbanks develop in fair weather conditions. It was also shown that suspended load tends to increase the growth rates of shoreface-connected ridges. However, the influence of the suspended load on the growth of tidal sandbanks has not been explicitly studied. From this study, we infer however that the suspension could have a large influence on the sandbank dynamics during storm periods.

[8] The largest influence of waves can be expected mainly in the nonlinear regime. Indeed, the work of *Huthnance* [1982] and *Roos* [2004] indicates that the effect of wind waves on the initial growth of tidal sandbanks is small; they mainly act on the final sandbank height and crest shape. Furthermore, case studies show a near absence of wave-induced structures on some sandbanks like the Middelkerke Bank [*Trentesaux et al.*, 1994].

[9] According to field observations in the southern North Sea [*Wentworth*, 1922; *Trentesaux et al.*, 1994; *van Lancker*, 1999], the grain size is not uniform and, over the sandbanks, ranges from 0.06 to 0.88 mm with a coarsening toward the crests. This coarsening has also been inferred from a linear stability analysis model [*Roos et al.*, 2007]. They show that in the model the preferred wavelength remains unchanged compared to the case of uniform sediment. The same type of behavior is found for the generation of tidal sand ridges [*Walgreen et al.*, 2004]: there is an increase of the growth and migration rates of tidal sand ridges for bimodal mixtures whereas the wavelength remain almost unchanged.

[10] On the basis of results from the studies above, we focus on the seabed dynamics for a bed load dominant transport, for the case of uniform sediment. On this basis, it appears that the most important processes for sandbank formation and their dependency on the grain size of uniform sediment are the tidal currents, the bed load and gravity driven sediment fluxes, and the particular sediment size. Thus, only these phenomena are taken into account in the following analysis.

2.2. Linear Stability Analysis Approach

[11] Following *Huthnance* [1982], we study the stability of a flat bed (h_0) subject to a current u_0 parallel to the x direction. For this purpose, the bed is perturbed by small amplitude bed forms defined by $h_1 = |h_1| \cos(kx + ly)$ (Figure 2). This bed perturbation induces the so-called first-order velocity ($\vec{u}_1 = (u_1, v_1)$) such that the current can

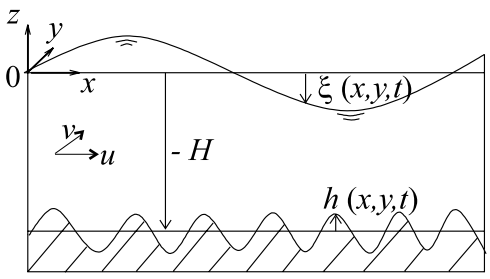

Figure 2. Sketch of the model geometry and related variables.

be written $\vec{u} = (u_0 + u_1, v_1)$. Depending on the perturbed hydrodynamics and the damping gravity-driven sediment flux [*Huthnance*, 1982], the bed perturbation will be damped or amplified. Using this approach, *Huthnance* [1982] obtained linear most amplified modes having wavelength and orientation corresponding to the sandbanks observed in the southern North Sea.

[12] Following his approach, the present model is based on the depth-integrated shallow water equations and takes into account only the bed load transport. The suspended sediment flux is neglected, according to the criteria proposed by *Van Rijn* [1989]. This criterion states that no sediment is transported by suspension if the sediment fall velocity is greater than the friction velocity. For example, for a 500 μm sediment diameter and a 1 m s^{-1} current in 30 m of water depth, the fall velocity is equal to 0.07 m s^{-1} whereas the friction velocity is equal to 0.03 m s^{-1}. For this case the suspension can be neglected. However, there are not many studies on the influence of suspension in the generation process. For finite amplitude bed forms, it seems that the main influence of suspension is on the equilibrium bank height and shape [*Roos*, 2004]. To avoid discrepancies, for modeling studies on real cases, the negligibility of suspension sediment flux with respect to the bed load sediment transport will be checked. If suspension is not negligible, then the model cannot be applied.

[13] Furthermore, neglecting the inertia of the fluid, we consider the stability of a bed subject to a schematized tidal current such that the current takes alternatively the value $-U$ and U during the tidal cycle. This implies that there is no migration of the bed perturbation. Technically, this analysis can be done using the stability analysis of a flat bed subject to a steady current. Indeed, *Fluit and Hulscher* [2002] show, by stability analysis, that the growth rate is the same for a bottom submitted to a block function alternate current and to a steady current.

[14] Within the stability analysis of this system, the first step is to compute the hydrodynamics induced by the bed perturbation. We use the steady shallow water equations, neglecting the viscosity terms and taking into account the Coriolis force. It is worthwhile to notice that this stability analysis is slightly different than the analysis performed in *Idier and Astruc* [2003]. Here, as a friction parameter, the Chézy coefficient is used, whereas the Strickler coefficient was used in the work of *Idier and Astruc* [2003]. This choice has been made in order to be consistent with the expression of the critical velocity based on the Chézy coefficient. The details of the mathematical procedure are presented in Appendix A. The hydrodynamic solution will be used for all the growth rate computations of this study.

2.3. Bed Evolution

[15] The bed evolution model is based on the sediment mass conservation equation

$$\frac{\partial z_b}{\partial t} + \frac{1}{1-p}\vec{\nabla}.\vec{S}_b = 0 \tag{1}$$

where $z_b = -H + h$ the bed level (H is mean bed level) defined in Figure 2, p is the bed porosity, and $\vec{S}_b$ is the sediment flux. For the bed load and gravity driven fluxes, a generic bed load formula can be written, for example, on the basis of the van Rijn formula:

$$\vec{S}_b = \alpha\left(|u|^2 - u_c^2\right)^b \left(\frac{\vec{u}}{|u|} - \lambda\vec{\nabla}h\right)\mathcal{H}(|u| - u_c) \tag{2}$$

where b is a coefficient (given in Table 1 for various formulae) and $\mathcal{H}$ is an Heaviside function such that sediment is transported only for sufficiently large velocity ($|u| > u_c$). The critical velocity u_c is computed using the critical sediment mobility parameter of Shields:

$$\theta_c = 0.047 = \tau_c/(\rho_s - \rho)gD_g \tag{3}$$

where τ_c is the critical bed shear stress and using the Chézy relationship:

$$\tau_c = \rho g u_c^2/C_h^2 \tag{4}$$

with a grain size–dependent Chézy coefficient (equation A4) and u_c, the critical velocity. In this study, the basic state velocity is equal to 1 m s^{-1}. From the above relation, this implies that particles having a diameter larger than 1.6 mm are not transported.

[16] In addition to the critical velocity, we notice that the bed slope coefficient λ, which is equal to the inverse of the tangent of the repose angle of sediment, is also grain size–dependent. From *van Rijn* [1989], the repose angle of 0.2 mm grains is about 38°, whereas it is 45° for 1 mm grains. These variations imply a bed slope coefficient λ equal to 1 for D_g = 0.2 mm and to 1.28 for D_g = 1 mm, i.e., a variation of 28% depending on the grain size. To take into account the grain size dependency, of the repose angle, we assume a linear variation of the repose angle (ϕ_r) with respect to the grain size D_g:

$$\phi_r(D_g) = 8750\left(D_g - 0.2 \times 10^{-3}\right) + 38 \tag{5}$$

Following the previous sandbank model [*Fluit and Hulscher*, 2002], we choose the *Meyer-Peter and Muller* [1948] formula, valid within the grain size range 0.4–1.6 mm. This formula leads to b = 1.5 and

$$\alpha = \frac{8\rho\sqrt{g}}{(\rho_s - \rho)C_h^3} \tag{6}$$

where ρ_s is the sediment mineral density (2650 kg.m^{-3}) and ρ is the water density.

2.4. Growth Rate Computation

[17] Following *Idier and Astruc* [2003], the stability analysis is performed in physical space. First, using the bed load formula (2) and splitting the velocity into zeroth-order and first-order components, the dimensional first-order sediment flux is

$$\vec{S}_{b1} = \frac{\alpha\rho g}{C_h^2}\frac{\left(|u_0|^2 - u_c^2\right)^{b-1}}{|u_0|}\left(2b - \frac{|u_0|^2 - u_c^2}{|u_0|^2}\right)(\vec{u}_0 \times \vec{u}_1)\vec{u}_0 + \frac{\alpha\rho g}{C_h^2}\left(|u_0|^2 - u_c^2\right)^b\left(\frac{\vec{u}_1}{|u_0|} - \lambda\vec{\nabla}h\right) \tag{7}$$

Table 1. Morphological Time Scale for Different Bed Load Formulas

Formula	Grain size Range Validity (mm)	a	b	α	T_m
MP-M, neglecting U_c	0.4–29	2	1.5	$\alpha = \frac{8\sqrt{g}}{(s-1)C_h^3}$	$T_m = \frac{(1-p)H}{\alpha\sigma U^2}$
MP-M, including U_c	0.4–29	2	1.5	$\alpha = \frac{8\sqrt{g}}{(s-1)C_h^3}$	$T_m = \frac{(1-p)HU}{\alpha\sigma\left(U^2-U_c^2\right)^{1.5}}$
VR (U_c including)	0.2–2	1	2.4	$\alpha = 0.005\ H^{-0.2}\ (s-1)^{-1.2}\ g^{-1.2}$	$T_m = \frac{(1-p)HU}{\alpha\sigma U(U-U_c)^{2.4}}$
E-H (no U_c)	0.2–4	2	2.5	$\alpha = \frac{0.08}{\sqrt{g}(s-1)^2 D_g C_h^3}$	$T_m = \frac{(1-p)H}{\alpha\sigma U^4}$

Furthermore, using the scaling (Table 2) and equations (1) and (2), we can define a morphological time scale T_m:

$$T_m = \frac{(1-p)HU}{\alpha\left(U^2 - U_c^2\right)^{1.5}\sigma} \tag{8}$$

The bed evolution equation can be written

$$\frac{\partial h_1}{\partial \tau} = \omega_g h_1 \tag{9}$$

where τ is a slow time variable such that $\tau = \hat{\alpha}\ t$ [*Fluit and Hulscher*, 2002]. Then, the dimensionless growth rate ω_g is

$$\omega_g = \underbrace{u_0\left(u_0^2 - \hat{u}_c^2\right)^{b-1} 2bk\frac{|u_1|}{|h_1|}\sin(\phi_u)}_{\omega_{g1}} + \underbrace{\left(u_0^2 - \hat{u}_c^2\right)^b\left[-\hat{\lambda}\left(k^2+l^2\right) + \frac{l|v_1|}{u_0|h_1|}\sin(\phi_v)\right]}_{\omega_{g2}} \tag{10}$$

In (10), the term ω_{g1} is a growth term, since the spatial phase lag ϕ_u (between the u component of the velocity and the bed perturbation) is positive (see Appendix A for the demonstration). The term ω_{g2} is a damping term due to the bed slope effect and the phase lag ϕ_v (between the v component of the velocity and the bed perturbation) which is negative (see Appendix A for the demonstration).

2.5. Grain Size Dependency

[18] In the model, the grain size–dependent dimensional parameters (C_h, α, U_c, λ) control on one hand the morphological time scale ($T_m = f(\alpha, U_c)$, equation (8)), and on the other hand the dimensionless growth rate ($\omega_g = f(\hat{r}, \hat{u}_c, \hat{\lambda})$, equation (10)) of each bed form. Indeed the velocity amplitude and phase (zeroth and first order) of equation (10) depends on the friction coefficient $\hat{r}$ (See equation (A13)).

[19] In order to study this grain size dependency, we consider the wavelength and the orientation of the linearly most amplified mode (LMA mode). Further a relevant output to study is the morphological time. Thus, using (9), we define a morphological doubling time (time needed for a bed form to have an amplitude two times larger than its initial amplitude) of the LMA mode such that

$$T_{m2} = \ln\ 2/\omega_g \tag{11}$$

3. Results and North Sea Application

3.1. Reference Case and Grain Size Dependency

[20] Here, we present the results obtained taking into account the grain size dependency of r, α, and u_c. This will be the reference case for the sensitivity analysis (section 4), chosen such that the results are comparable to previous stability analyses which used physical parameters assumed to be representative of the North Sea [*Hulscher et al.*, 1993; *Idier and Astruc*, 2003]. The physical parameters are a water depth H of 30 m, a current magnitude of 1 m s^{-1} and a grain size of 0.5 mm. The dimensional growth rate ($=\hat{\alpha}\omega_g$) is plotted in Figure 3a for this case. We observe a band of amplified modes. The linearly most amplified mode has a wavelength of 11.5 km and an orientation of $-39.7°$, relative to the current $\vec{u}_0$, i.e., a counterclockwise orientation due to the Coriolis force.

[21] Within the range 0.4–1.6 mm, Figures 4a and 4b show that the wavelength of the linearly most amplified mode decreases from 12 to 5 km for increasing grain size, whereas the orientation decreases from -40.4 to $-37.8°$. Thus, the grain size has a negligible influence on the bed form orientation whereas it leads to wavelength variations of the LMA mode of a factor 2. This could explain why, within a group of sandbanks, even if there are changes of grain size in the offshore-onshore direction, the sandbank orientation remains quite uniform within the sandbank group. The morphological doubling time increases from 200 to 4×10^5 years (Figure 4c).

[22] The present model gives quite a large morphological time with values ranging from 215 to 700 years (Figure 4c). This means that these bed forms would need several centuries to grow and reach their finite amplitude stage. These growth rates are in accordance with the results of *Idier and Astruc* [2003] where the generation and the saturation time have been studied. They show that such sandbanks would need about 8000 years to reach their finite amplitude stage. They also explained, on the basis of geological studies, that the North Sea sandbanks should be about 8000 years old. On this time scale the mean sea level has significantly changed (+30 m). Using a composite modeling approach, *Idier* [2002] studied the long-term behavior of sandbanks taking into account these sea level variations and showed that sandbanks grow quite quickly at the beginning (for a small water depth), and then the sandbank height follows the sea level variations.

3.2. Norfolk Sandbanks

[23] In *Besio et al.* [2006], one of the field areas which was used for model validation was the coastal region of the

Table 2. Dimensionless Parameters[a]

Parameter	Definition
$\hat{r}$	$gU/C_h^2\sigma H$
$\hat{\lambda}$	$\lambda H\sigma/U$
$\hat{\alpha}$	$\alpha(U^2 - U_c^2)^b/HU$
$\hat{f}$	f/σ

[a]The scaling quantities are the velocity U (1 m/s), the water depth H (30 m), and the tidal frequency σ (1.4×10^{-4}s^{-1}).

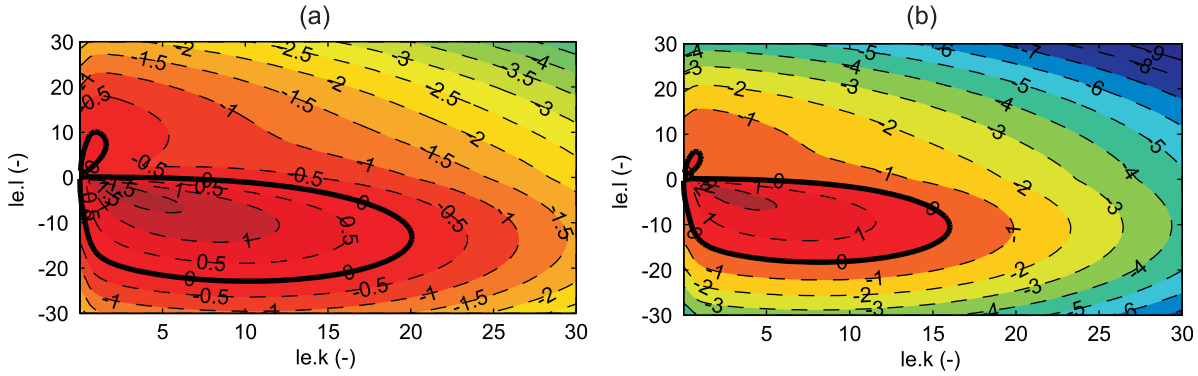

Figure 3. Dimensional growth rate (a^{-1}) versus ($l_e k$, $l_e l$), where l_e is the tidal excursion length ($l_e = U/\sigma$) for D_g = 0.5 mm. (a) $U_c = f(D_g)$. (b) $U_c = 0$.

Norfolk Banks [*Collins et al.*, 1995]. In this area, the observed sandbank wavelength ranges between 4 and 10 km. The model of *Besio et al.* [2006] is based on a 3-D stability analysis, and the physical processes that are taken into account are slightly different (3-D hydrodynamics, suspension transport, tidal current ellipticity are taken into account whereas they are not considered in the present study). They obtained a sandbank wavelength of 5.5 km. We use the same representative physical parameters as *Besio et al.* [2006]: water depth of 30 m, currents of 0.7 m s^{-1}, and a grain size of 0.15 mm. Using the same seabed roughness of 5 cm, a wavelength of 4.4 km is obtained (Figure 5a), which is consistent with the observations and the 5.5 km obtained by *Besio et al.* [2006]. Taking into account the grain roughness only (form roughness is neglected), a wavelength of 6.6 km is obtained (Figure 5b). Thus, whatever the sea bed roughness, for this area, the occurrence and the magnitude of the wavelength are consistent with the model of *Besio et al.* [2006] and with the observations. Thus, we continue from there and investigate the occurrence of sandbanks and their wavelength at the North Sea scale.

3.3. Entire North Sea

3.3.1. GIS Data

[24] Location specific parameters are used as model input which results in location specific predictions for the occurrence of sand banks. The tidal data are provided by RIKZ (Rijksinstitut voor kust en zee, now part of Deltares) and obtained using a model (ZUNOWAQ) [*Verlaan et al.*, 2005], here we used the M2 component. The grain size data are digitized from geological maps from the Dutch, British and Belgian Hydrographical Services [*Balson et al.*, 1991; *Cameron et al.*, 1984; *Harrison et al.*, 1987]. Additional data on the grain size for the Dutch part of the North Sea were provided by TNO-NITG. The water depth is taken from the boundary conditions of the ZUNOWAQ model [*Van den Brink*, 1998]. These location-specific data are displayed in a GIS. Figure 6 shows the values of these three parameters over the North Sea.

[25] In order to apply the model in an area where we can be confident of the model validity in terms of sediment transport mode, the bed load (q_b) and suspension sediment fluxes (q_s) are computed using the formulation of *van Rijn* [1989] and compared in Figure 7. We choose the condition $q_b/q_s > 1\%$ as a threshold above which the model is valid. It can already be noticed that the area where the suspension is assumed negligible is quite similar to the sandbank area (Figure 1).

3.3.2. Model Versus Observations

[26] Figure 8a shows the predicted wavelength obtained using a grain roughness. The grain roughness is computed on the basis of the grain size data in the GIS database, and thus is not uniform over the North Sea. In the GIS database, we do not have a map of the observed wavelength. What we know at the North Sea scale is the location of the sandbank crests (Figure 1). As shown by *Knaapen* [2008] on the Dutch continental shelf, it is possible that sandbanks occur more widely than is known today. In addition to the occurrence, wavelengths between 2 and 10 km are inferred in the North Sea from the field data [*Off*, 1963]. Thus, first, comparing Figures 1 and 8a, we notice that the model is able to predict the occurrence of sandbanks correctly. The main area of difference is located in the north east sector of the North Sea, along the Dutch coast. The wavelength model prediction mainly ranges between 2 and 10 km, which is in accordance with *Off* [1963].

[27] In order to better quantify the influence of the critical velocity on the results, the critical velocity is switched off, and the model is applied again to the North Sea. Figure 8b shows that neglecting the critical velocity leads to sandbank occurrence wherever in the North Sea the model is applied. So, the model predicts a much more extensive occurrence than when the critical velocity is taken into account. For the area where sandbank occurrence is predicted by the model, the sandbanks are more or less two times larger (Figure 8b) than when the critical velocity is taken into account (Figure 8a). Also, in the north of the study area, there are very long wavelengths reaching 50 km, which seems quite unrealistic.

[28] It is quite difficult to quantify the model errors in comparison with the North Sea field observations because of the lack of a sufficiently detailed map of sandbank occurrence and wavelength. However, taking into account all the grain size dependencies significantly changes the prediction of sandbank occurrence and wavelength, and thus should be taken into consideration for future study.

3.3.3. Model Sensitivity

[29] In the results presented in Figure 8a, two assumptions have been made: one on the area of validity of the model (area where bed load is dominant), and one on the bed roughness (taken equal to the grain roughness).

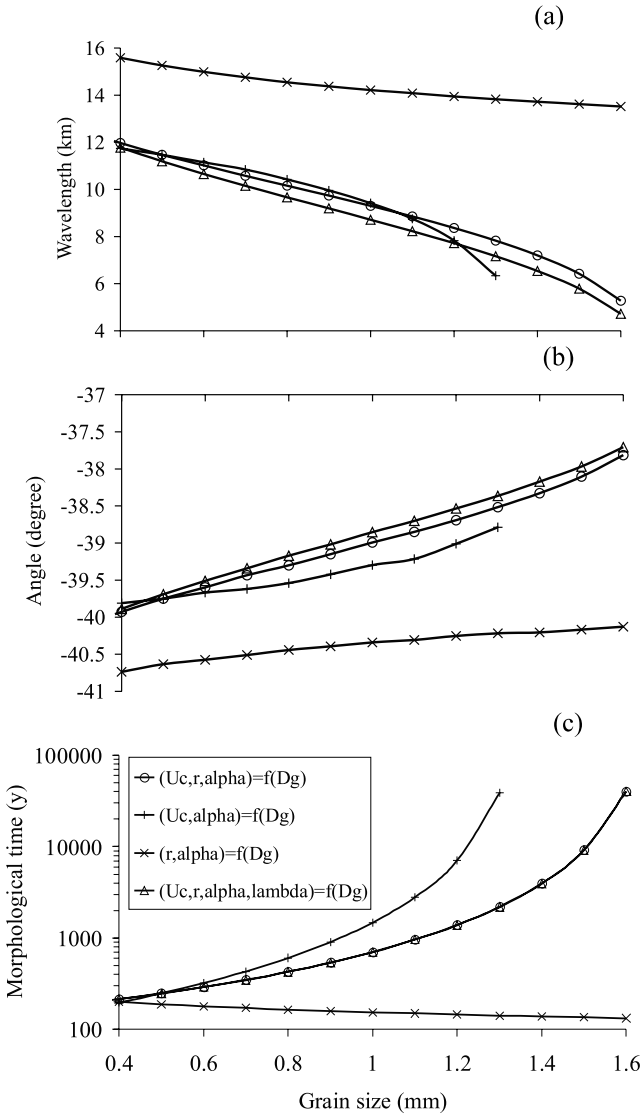

Figure 4. Characteristics of the linearly most amplified mode (from the linear stability analysis) versus the grain size: (a) wavelength, (b) crest orientation relative to the current, (c) morphological doubling time. Four cases are plotted depending on the grain size–dependent parameters which are taken into account: (U_c, r, α), (U_c, α), (r, α), and (U_c, r, α, λ). When these parameters are not varying with the grain size, the default values for r and λ are those for a grain size of 0.5 mm, and the default value of U_c is zero.

[30] First, the condition of application of the model is switched off, and the model is applied to the whole North Sea whatever the suspension fluxes (Figure 9a). With this approach, there would be sandbanks in a larger part of the North Sea, including areas where no sandbanks are observed (e.g., in the middle of the North Sea). According to *Knaapen* [2008], the fact that no sandbanks have been observed in this central part does not mean that there are no sandbanks. Regarding the area along the northern Dutch coast, the results of switching off the condition of the bed load dominant mode does not improve the results: no sandbanks are predicted in this area.

[31] Second, we use a constant bed roughness (k_s of 0.02 m) and retain the condition on the bed load sediment flux versus the suspension fluxes ($q_b/q_s > 1\%$). Figure 9b shows the wavelength of the generated patterns. Compared to the case in which only the grain bed roughness is taken into account (Figure 8a), the wavelength are quite similar. The main difference is in the occurrence: the area of sandbanks is larger if full bed roughness (including ripples) is taken into account. The results are quite improved, with a better prediction of sandbank occurrence along the northern Dutch coast (Figure 1). Thus, it appears important to take into account this parameter for application in real cases.

[32] It is possible to explain the difference in the results taking into account only grain roughness or a ripple induced roughness. Looking at the influence of the bed roughness on the critical velocity, which determines if there is sediment transport or not, we note that the critical velocity (equations (3) and (4)) can be written

$$u_c = C_h\sqrt{0.047 D_g \rho_s/\rho} \tag{12}$$

Increasing the bed roughness leads to a decrease of the 2DH critical velocity. Figure 10 shows the area of model application ($q_b/q_s > 1\%$ and $U > U_c$) for the case in which (1) only the grain roughness is taken into account and (2) uniform ripple roughness is taken into account. The bed roughness induces an increase of the area of application of the model. This is the same coverage as can be seen in Figure 9b. Thus, the influence of bed roughness on sandbank generation in the North Sea would be mainly on the sandbank occurrence rather than on the wavelengths.

4. Discussion on the Grain Size Dependency

4.1. Sensitivity Study

[33] In order to identify, for a simple case, which of the four grain size–dependent parameters has the largest effect, and on which sandbank characteristic (morphological time, geometrical property), we successively switch off the these parameters and compare the results with the reference case (Figure 4, (Uc,r,α,λ) = f(Dg)).

4.1.1. Bed Slope Effect (λ Parameter)

[34] The grain size dependency of the bed slope effect is switched off such that the default value of the parameter λ corresponds to a repose angle of sediment of 38°. This value falls within the range of the observed repose angles (30 to 40°, *van Rijn* [1989]). Figure 4 ((Uc,r,alpha) = f(Dg)) shows that neglecting the variation of the grain size dependency of the bed slope effect does not significantly change the results obtained if it is not neglected.

4.1.2. Friction (r)

[35] To study the influence of the grain size dependency in the friction on the sandbank generation, we use the reference case based on the Meyer Peter and Muller (MP-M) formula, including the critical velocity, and switch off the grain size dependency of this coefficient. We notice that freezing the friction coefficient has an influence on the critical velocity, through equation (4). The friction coefficient is frozen to $\hat{r} = 0.249$, corresponding to the friction coefficient for a grain size of 0.5 mm.

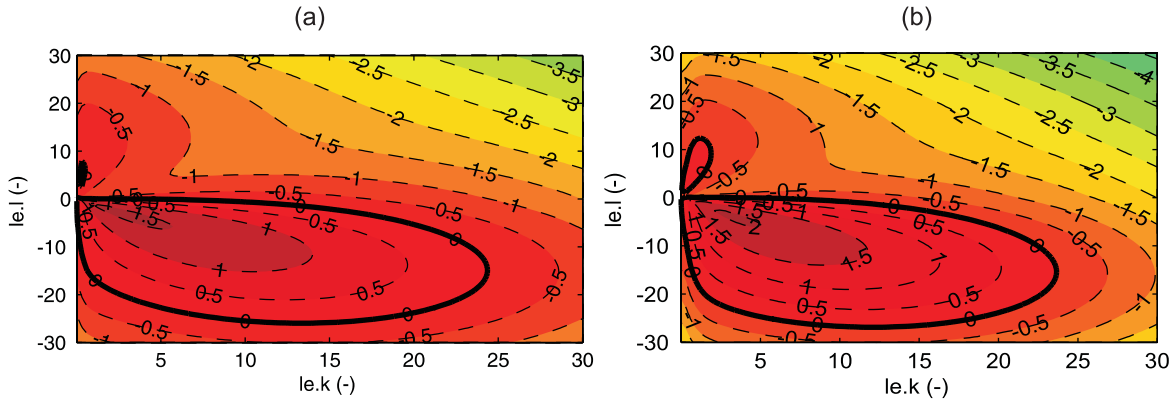

Figure 5. Dimensional growth rate (a^{-1}) versus ($l_e k$, $l_e l$), where l_e is the tidal excursion length ($l_e = U/\sigma$) for D_g = 0.150 mm, U = 1 m/s, H = 30 m for (a) a grain roughness and (b) a bed roughness of 5 cm.

[36] Figure 4 (case (Uc,alpha) = f(Dg)) shows the influence of freezing the friction term on the geometry and morphological time of the linearly most amplified (LMA) mode. First, we notice that the computations have been done for a grain size smaller than 1.4 mm. Indeed, for D_g = 1.4 mm, the critical velocity obtained through (4) is larger than 1, i.e., larger than the ambient current, and no real solution can be found. For this grain size range, Figures 4a and 4b show that freezing this coefficient has a small influence on the geometrical properties of the LMA mode. Figure 4c shows that freezing this coefficient has a strong influence on the morphological time, with a morphological time two times larger (1475 a) than for the case in which the friction coefficient is not frozen, and thus grain size–dependent (700 a).

[37] Thus, the grain size dependency of the friction coefficient has a relatively small impact on the sandbank geometry, but a rather large effect on the morphological time scale: for the studied case, it leads to variations of 100%.

4.1.3. Morphological Time Scale (T_m)

[38] Several bed load formulae have been tested: Meyer-Peter and Muller (MP-M) [*Meyer-Peter and Muller*, 1948], van Rijn (VR) [*van Rijn*, 1984] and Engelund-Hansen (E-H) [*Engelund and Hansen*, 1967]. From equations (6) and (8) and Table 1, the main influence of the choice of the bed load formula is on the morphological time scale (T_m). The morphological time scale T_m is equal to $1/\hat{\alpha}\sigma$ (and $\hat{\alpha} = \alpha(U^2 - U_c^2)^b/HU$, Table 2). Thus the grain size dependency of the morphological time scale is controlled by following grain size–dependent parameters: the α coefficient and the critical velocity U_c.

[39] Figure 11 shows the variations of the coefficient α versus the grain size for the MP-M, VR, and E-H bed load formulae. It is shown that the coefficient behavior is different for each bed load formula. For the VR formula, the coefficient is constant with respect to grain size. For the other formulae, it varies with a maximum factor of 2 (see Table 1 for the formulation of the MP-M and E-H α coefficient). The dimensionless equations of the system are independent of the coefficient α. Thus, the grain size dependency of the sedimentary coefficient α controls the result only through the morphological time scale T_m (equation (8)) and has no influence on the geometrical properties of the LMA mode.

[40] The critical velocity is the other parameter controlling the grain size dependency of the morphological time scale. Thus, the critical velocity is switched off in the MP-M bed load formula. Figure 12 shows the grain size dependency of the morphological time scale depending on the bed load formulae and for the cases where the critical velocity is taken into account or switched off. It shows that the morphological time scale ranges between 56 (VR, Uc = 0) and 10,000 years (MP-M, Uc included), thus, the influence of the critical velocity and its grain size dependency is quite large.

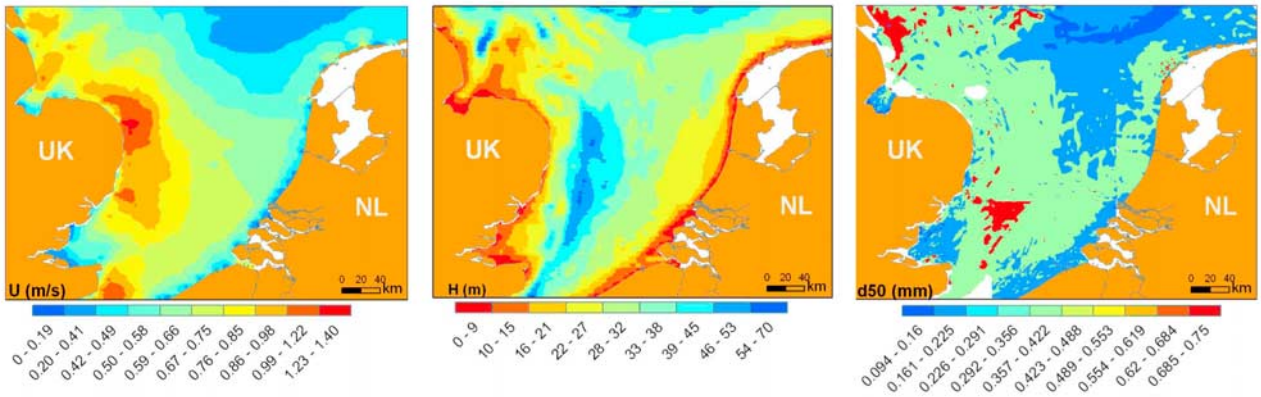

Figure 6. GIS data: flow velocity (m s^{-1}), water depth (m), and grain size (m).

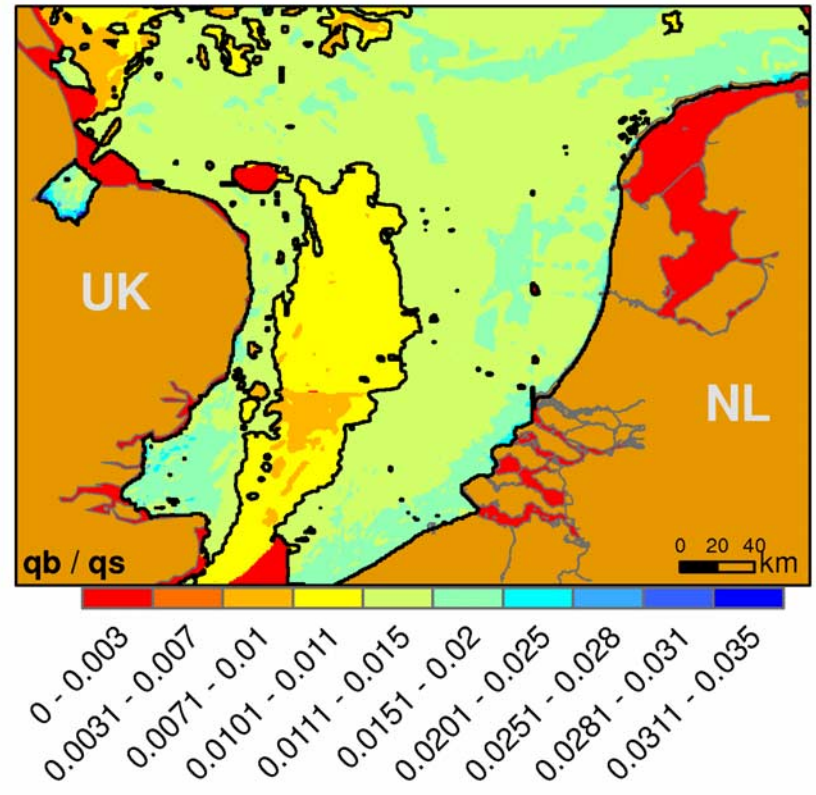

Figure 7. Bed load sediment flux divided by the suspension sediment flux. The contour line indicates the limit $q_b/q_s = 0.011$.

[41] To estimate the influence of the bed load formula choice (which depends on the morphological time scale), two other formulae are investigated (VR and E-H). Figure 12 shows a wide range of morphological time scales, depending on grain size and bed load formula. The morphological time scale ranges between 200 (E-H) and 10,000 years (MP-M and VR). The time scale ranges from 200 (E-H) to about 550 (MP-M) years for a grain size of 0.4 mm and from

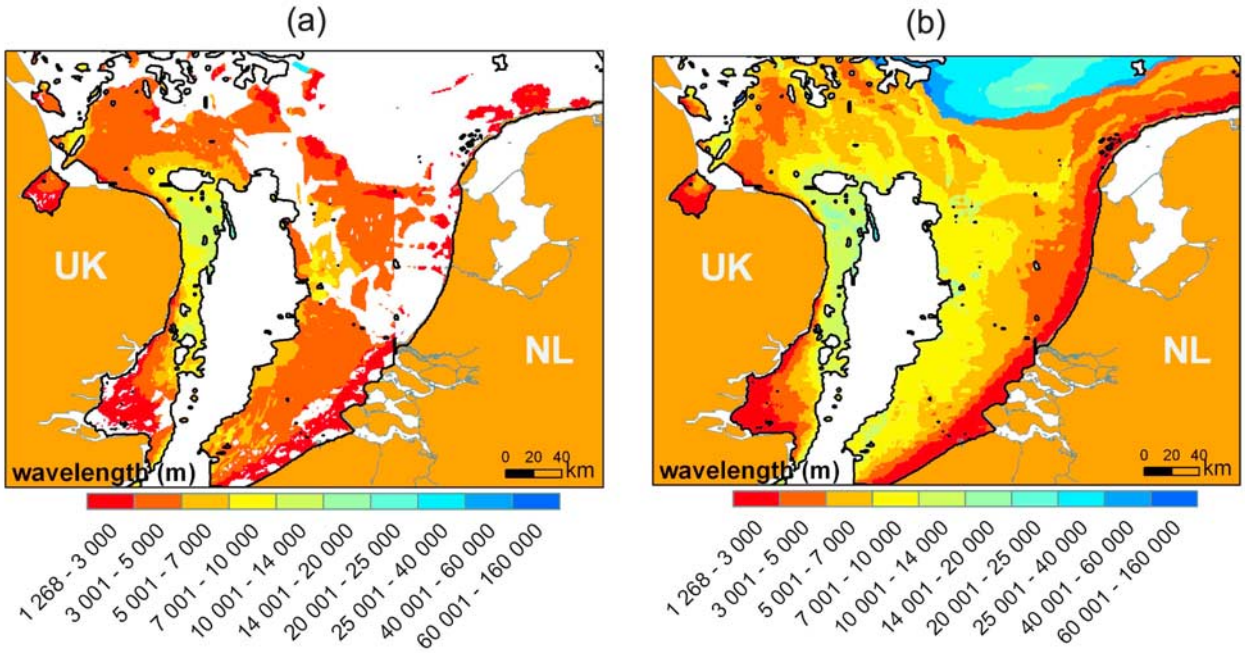

Figure 8. Sandbank wavelength predicted by the model in the bed load dominant area ($q_b/q_s > 1\%$) (a) taking into account u_c and (b) neglecting u_c.

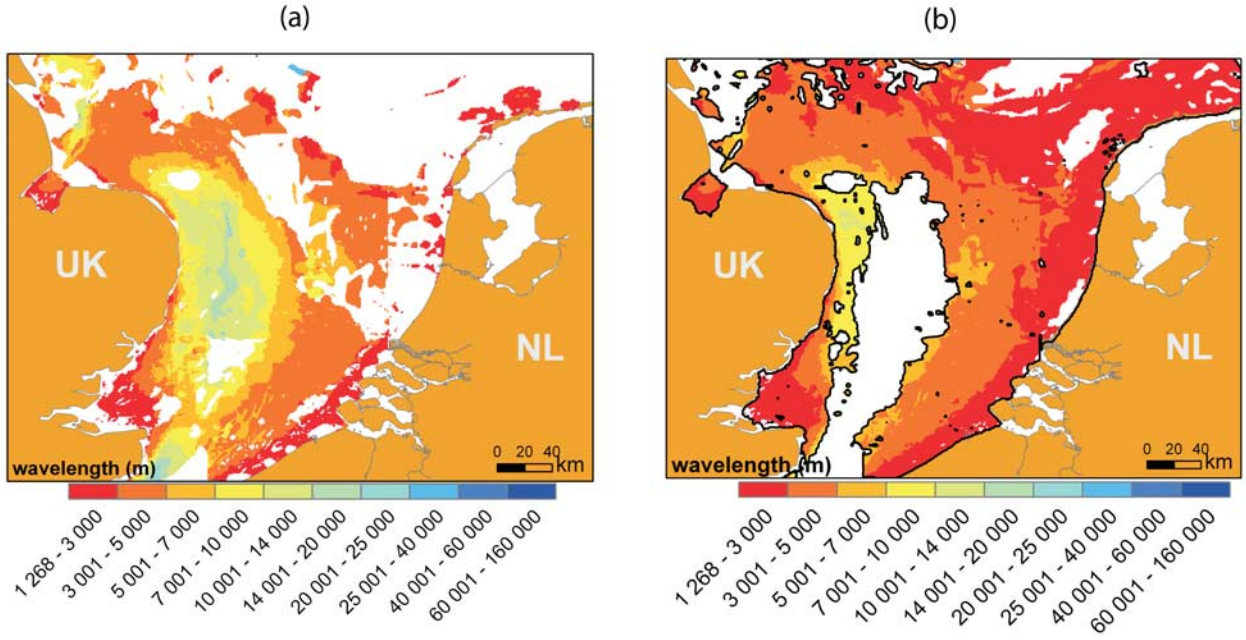

Figure 9. Sandbank wavelength predicted by the model compared to the reference case (Figure 8a) (a) neglecting the dominant bed load condition (q_b/q_s > 1%) and (b) taking into account a uniform bed roughness of k_s = 0.02 m.

550 (E-H) to 10,000 (MP-M) years for a grain size of 1.5 mm.

[42] We note that the formula of E-H does not include any critical velocity and thus, could be used without any further development. Furthermore, the comparison of the MP-M (Uc = 0), VR and E-H formulae (Figure 12) shows that around a grain size of 0.5 mm, the differences on the morphological time scale are negligible with a time scale of about 300 years for the chosen parameters. Thus, the previous analyses [*Fluit and Hulscher*, 2002; *Idier and Astruc*, 2003] which were performed for a grain size of 0.5 mm and the MP-M formula (Uc = 0) should provide results with a morphological time scale comparable to the results of the present paper for the 0.5 mm case.

4.1.4. Critical Velocity (U_c)

[43] As shown above, the critical velocity influences both the morphological time scale and the dimensionless growth rate. To investigate the influence of this parameter, we switch it off (case (r,α) = f(Dg)).

[44] First, equation (10) shows that, for fixed wavelength and orientation, switching off the critical velocity leads to a larger growth rate, and thus a smaller morphological time. Figure 3b shows the dimensional growth rate for a grain size of 0.5 mm. Neglecting the critical velocity, the most amplified mode has a wavelength of 15.5 km and an orientation of −41.5°, relative to the current. Taking into account the critical velocity the wavelength and the orientation are respectively equal to 11.5 km and −39.7°. Thus, taking into account the critical velocity results in sandbank wavelengths

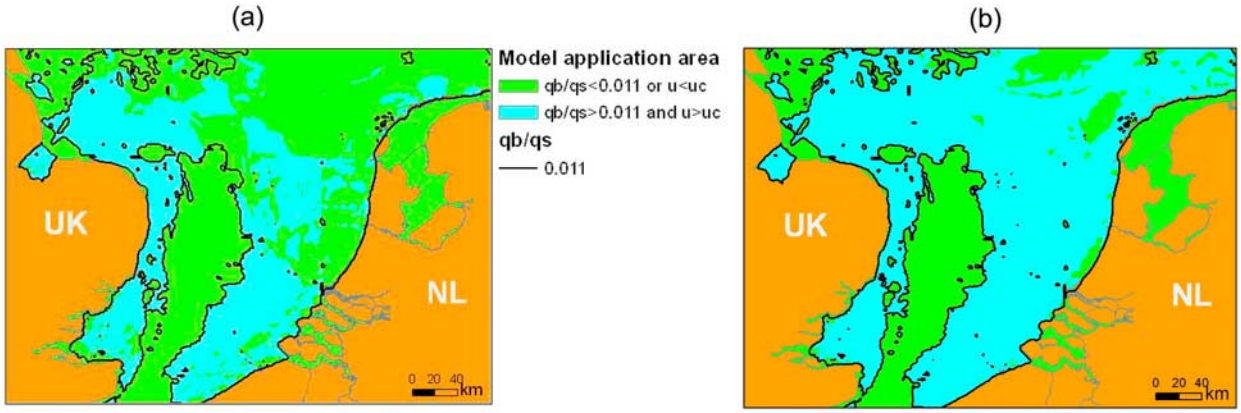

Figure 10. Area of model application for q_b/q_s > 1% and $u > u_c$ for (a) a nonuniform grain roughness and (b) a uniform ripple roughness of ks = 2 cm.

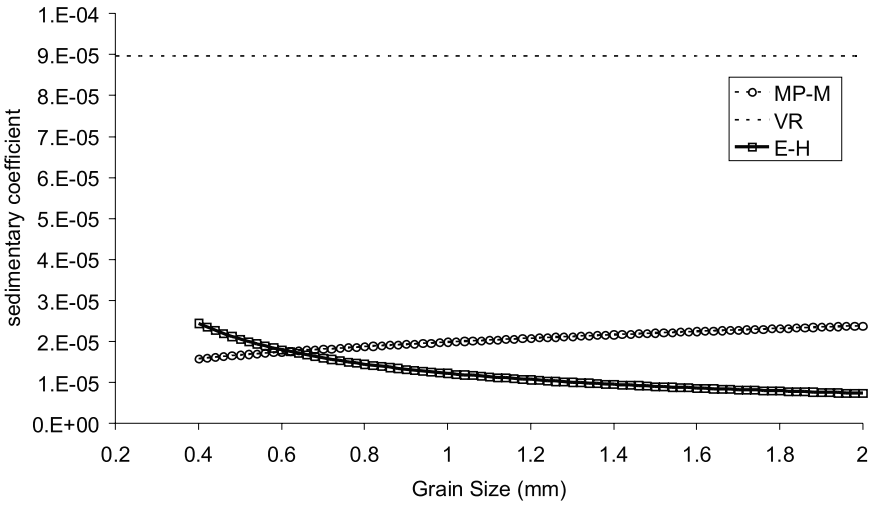

Figure 11. Sedimentary coefficient α versus the grain size for several bed load formula (MP-M, Meyer-Peter and Muller; VR, van Rijn; E-H, Engelund-Hansen). The curves are plotted in their grain size validity range.

more consistent with the observed values (several kilometers, up to about 10 km) than the wavelength of 15.5 km obtained if the critical velocity is neglected.

[45] Figure 4a shows that, for the grain size range 0.4–1.6 mm, the wavelength varies from 16 km to 13.5 km if the critical velocity is neglected. The angle between the crest and the current varies from -41.0 to $-40.1°$ (Figure 4b). Thus, for both cases (critical velocity taken into account or not), the grain size has a negligible influence on the bed form orientation. Regarding the wavelength, the grain size dependency is larger if the critical velocity is taken into account (variation of a factor 2 against a factor 1.3).

[46] The morphological doubling time (equation (11)) decreases from 200 to 132 years for grain size increasing from 0.4 to 1.6 mm (Figure 4c). If the critical velocity is taken into account (case (Uc,r,α) = f(Dg)), the morphological doubling time increases. Thus, neglecting the grain size dependency of the critical velocity lead to an opposite variation of the morphological doubling time. The discrepancies in the doubling time increase with the grain size. Figure 4c shows that taking into account the critical velocity leads to a doubling time increase of 24% for a grain size of 0.5 mm and 78% for a grain size of 1 mm. Even a calibration for one grain size will not decrease the discrepancies since these two grain size–dependent doubling times have opposite tendencies. Between the two tendencies, the increase of the doubling time with the grain size obtained if the critical velocity is taken into account seems more reasonable than a decrease. Thus, in studies of morphological time or grain size dependency, taking into account the critical velocity should significantly diminish the errors, even for medium sands.

4.2. Analysis of the Critical Velocity Influence

[47] In this section, the differences in effects for including a critical velocity are analyzed. Taking into account the

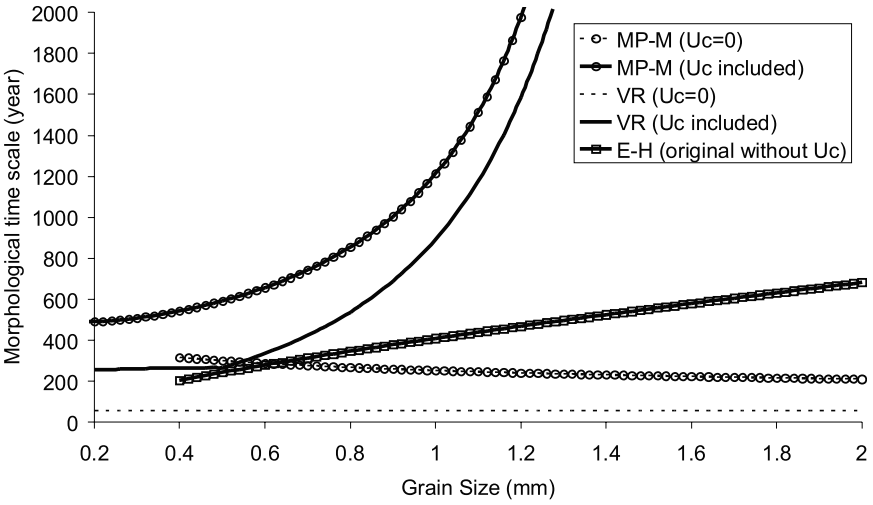

Figure 12. Morphological time scale versus the grain size for several bed load formula (same as Figure 11). The curves are plotted in their grain size validity range.

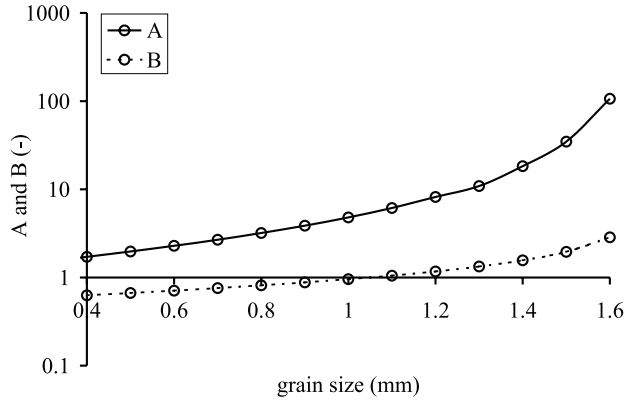

Figure 13. Terms A and B (equation (14)).

critical velocity leads to a decrease of both the growth term ω_{g1} and the damping term ω_{g2} (equation (10)) and the balance between growth and damping terms is modified. Indeed, the following relationship can be written

$$\frac{\omega_{g1}\left(u_c = f\left(D_g\right)\right)}{\omega_{g2}\left(u_c = f\left(D_g\right)\right)} = \frac{u_0^2}{u_0^2 - u_c^2}\,\frac{\omega_{g1}(u_c = 0)}{\omega_{g2}(u_c = 0)} \tag{13}$$

Then, if the grain size increases, the critical velocity increases, the quantity $u_0^2/(u_0^2 - u_c^2)$ decreases. Thus the growth term ω_{g1} is relatively larger compared to the damping term ω_{g2} when the critical velocity is taken into account, even more so for large grains. This implies that small wavelengths which were damped for a zeroth-order critical velocity could now be amplified (Figure 3) and the wavelength of the linearly most amplified mode (LMA mode) becomes shorter. Regarding the doubling time, some information can also be provided. First, coming back to the dimensional space and considering the morphological time scale T_m, the following relationship between the doubling times can be written

$$\frac{T_{m2}\left(u_c = f\left(D_g\right)\right)}{T_{m2}(u_c = 0)} = \underbrace{\frac{T_m\left(u_c = f\left(D_g\right)\right)}{T_m(u_c = 0)}}_{A}\,\underbrace{\frac{\omega_g(u_c = 0)}{\omega_g\left(u_c = f\left(D_g\right)\right)}}_{B} \tag{14}$$

Both terms A and B lead to an increase of the doubling time if the critical velocity is taken into account (Figure 13). However, the term A, resulting from the scaling, is much larger than the term B. Thus, the variations in the doubling time are mainly due to the scaling of the bed evolution equation, i.e., the scaling of the bed load transport formula (2). Then, for a uniform sediment cover, previous studies [e.g., *Huthnance*, 1982] that neglect the critical velocity could be used with a correction of the morphological time scale variations with the grain size.

5. Conclusions

[48] In this study, the grain size influence in sandbank generation dynamics has been studied through a modeling approach. A 2DH stability analysis model, including most of the grain size–dependent parameters is developed for the case of a uniform sediment bed subject to tidal currents, bed load and gravity-driven sediment fluxes.

[49] The model is applied to the North Sea. A sensitivity study is carried out for this area and the results are compared to available observations of sandbank occurrence. The results show that (1) including the critical velocity and its grain size dependence improves the results in terms of sandbank wavelength prediction, (2) excluding the area where suspension sediment transport is not negligible improves the results in terms of sandbank occurrence, and (3) taking into account a uniform ripple related bed roughness improves the results in terms of sandbank occurrence. The linear model, which initially includes the critical velocity, is thus applied taking into account the area of the model validity (bed load dominant) and the ripple roughness, and gives results in terms of sandbank occurrence and wavelength which are consistent with the field observations.

[50] Using the model, we investigated the influence of grain size–dependent parameters on the geometrical and temporal properties of small amplitude sandbanks. The results show that (1) the grain size dependency of the bed slope effect has a negligible influence on geometrical and temporal properties, (2) the friction coefficient has a negligible influence on the geometrical properties but strongly affects the morphological time scale, (3) the morphological time scale (through the bed load formula choice) is strongly influenced by the grain size, and (4) the critical velocity strongly affects the geometrical and temporal properties of sandbank predictions.

[51] Thus, this study shows that the critical velocity is the most important parameter to take into account. Neglecting this critical velocity leads to a morphological time having a grain size dependency opposite to the dependency obtained if this critical velocity is taken into account: in the first case the morphological time decreases with the grain size, whereas in the second case, it increases. The consequences on the geometrical properties of the bed forms are less drastic, with a variation of 25% for the wavelength of the linearly most amplified mode, for a grain size of 0.5 mm.

[52] Within the present study, some similarities have been observed between the area of dominant bed load ($q_b/q_s > 1\%$) and the known sandbank occurrence in the North Sea. In order to better understand the sandbank generation processes, and also to extend the model validity, it would be worthwhile to include suspension in the model.

Appendix A: Hydrodynamic Computation

[53] Within the stability analysis of this system, the first step is to compute the hydrodynamics induced by the bed perturbation. The steady shallow water equations can be written as follows, neglecting the viscosity terms:

$$u\frac{\partial u}{\partial x} + v\frac{\partial u}{\partial y} = -g\frac{\partial \xi}{\partial x} - \frac{g\sqrt{u^2+v^2}}{C_h^2(H+\xi-h)}u + Fv \tag{A1}$$

$$u\frac{\partial v}{\partial x} + v\frac{\partial v}{\partial y} = -g\frac{\partial \xi}{\partial y} - \frac{g\sqrt{u^2+v^2}}{C_h^2(H+\xi-h)}v - Fu \tag{A2}$$

$$\frac{\partial}{\partial x}[(H+\xi-h)u] + \frac{\partial}{\partial y}[(H+\xi-h)v] = 0 \tag{A3}$$

where (u, v, h, ξ) is defined in Figure 2, g is the gravity acceleration (9.81 ms^{-2}), H is the mean water depth (30 m), f is the Coriolis coefficient equal to 1.1×10^{-4} rd.s^{-1}, for a latitude of 50° (southern North Sea), and C_h is the Chézy friction coefficient. In these equations, the grain size dependency is taken into account through the Chézy coefficient:

$$C_h = 18 \log \frac{12H}{3D_g} \tag{A4}$$

where D_g is the grain size. Here, only one grain size is considered, such that there are no differences between the commonly used D_{50}, D_{90}, and D_g.

[54] Assuming a negligible free surface slope, the first-order fluid velocity components u_1 (resp. v_1), resulting from the sinusoidal seabed perturbation h_1, can be written as a sinusoidal function in horizontal space such that $u_1 = \cos(kx + ly + \phi_u)$ (resp. $v_1 = \cos(kx + ly + \phi_v)$). A positive phase lag ϕ_u (resp. ϕ_v) means that the velocity maximum is located upstream the bed form crest. In order to solve the system, the equations (A1), (A2), and (A3) are scaled following *Fluit and Hulscher* [2002]:

$$\vec{u} = U u_* \quad ; \quad \vec{x} = l_m x_* \quad ; \quad t = \frac{t_*}{\sigma} \quad ; \quad h = H h_* \quad ; \quad xi = \frac{U l_m \sigma}{g} \xi_* \tag{A5}$$

where σ is the tidal frequency (1.4×10^{-4} s^{-1} for an M2 tide), L is the tidal wavelength ($L = \sqrt{gH}/\sigma$), l_m is the length of the tidal excursion ($l_m = U/\sigma$), H is the mean water depth, and U is the magnitude of the current. The asterisks indicate the dimensionless quantities. In what follows, the asterisks are dropped for reading convenience. This procedure leads to the dimensionless parameters defined in Table 2: the friction parameter $\hat{r}$, the bed slope effect parameter $\hat{\lambda}$, the sedimentary parameter $\hat{\alpha}$, and the Coriolis effect parameter $\hat{f}$.

[55] We assume that μ is a small parameter related to the dimensionless amplitude of the bed perturbation imposed on the flat bottom (μ is the ratio between the bed perturbation amplitude and the water depth). In the present study, we focus on the generation, thus on perturbation such that $\mu < 1$. If the exact solution of the problem is $\phi = (\xi, u, v, h)$, then, the solution can be written

$$\phi = \phi_0 + \mu\phi_1 + \mu^2\phi_2 \tag{A6}$$

The zero-order solution which describes the flow over a flat bottom is ϕ_0 ($h_0 = 0$); ϕ_1 is the first-order solution. After some algebra, the solution ϕ_0 satisfies $\phi_0 = (-\hat{r}C^2, C, 0, 0)$, with C a constant [*Idier and Astruc*, 2003]. C is equal to the dimensionless basic current velocity and thus can be taken equal to 1 in what follows. This solution describes a steady uniform flow along the x direction, over a flat bed. The sediment transport is also uniform, such that the bed level remains flat.

[56] Using the zeroth-order solution, the first-order solution comes from the following system:

$$\frac{\partial \xi_1}{\partial x} + \frac{\partial u_1}{\partial x} + \hat{r}(2u_1 + h_1) - \hat{f}v_1 = 0 \tag{A7}$$

$$\frac{\partial \xi_1}{\partial y} + \frac{\partial v_1}{\partial x} + \hat{r}(v_1) + \hat{f}u_1 = 0 \tag{A8}$$

$$\frac{\partial u_1}{\partial x} + \frac{\partial v_1}{\partial y} = \frac{\partial h_1}{\partial x} \tag{A9}$$

The system is written as a function of h_1, in the spectral space such that the unknowns are Fourier transformed:

$$\phi_1 = \int\int \tilde{\phi}_1\left(\vec{k}, t\right) e^{-i\vec{k}.\vec{x}} d\vec{k} + cc \tag{A10}$$

where cc is the conjugate, $i^2 = -1$, and $\vec{k} = (k, l)$ is the two-dimensional wave vector. Then, the system can be written in matrix form, in the Fourier space (denoted by $\tilde{\phi}$):

$$\begin{bmatrix} -ik & -ik + 2\hat{r} & -\hat{f} \\ -il & \hat{f} & -ik + \hat{r} \\ 0 & -ik & -il \end{bmatrix} \begin{bmatrix} \tilde{\xi}_1 \\ \tilde{u}_1 \\ \tilde{v}_1 \end{bmatrix} = \tilde{h}_1 \begin{bmatrix} -\hat{r} \\ 0 \\ -ik \end{bmatrix} \tag{A11}$$

Solving leads to

$$\tilde{u}_1 = \tilde{h}_1 \frac{\hat{r}(l^2 - k^2) + ik^3 - kl\hat{f}}{-\hat{r}(k^2 + 2l^2) + ik(k^2 + l^2)} \tag{A12}$$

$$\tilde{v}_1 = \tilde{h}_1 k \frac{-3\hat{r}l + ikl + k\hat{f}}{-\hat{r}(k^2 + 2l^2) + ik(k^2 + l^2)} \tag{A13}$$

The velocity module $|u_1|$ (resp. $|v_1|$) is equal to $|\hat{u}_1|$ (resp. $|\tilde{v}_1|$), whereas the phase lag ϕ_u (resp. ϕ_v) is such that $\phi_u = -\arctan \Im(\hat{u}_1)/\Re(\hat{u}_1)$ (resp. $\phi_v = -\arctan \Im(\tilde{v}_1)/\Re(\tilde{v}_1)$). $\Re$ and $\Im$ are respectively the real and imaginary part of the complex variable. From this analytical solution (A13), after some algebra, it can be seen the phase lag ϕ_u is always positive, whereas the phase lag ϕ_v is always negative (A13).

Notation

α	Sedimentary coefficient [depends on the bed load formula].
C_h	Chézy coefficient [m$^{1/2}$ s^{-1}].
D_g	Grain size [m].
f	Coriolis coefficient [N m^{-1} s^{-1}].
ϕ_u	Spatial phase lag between the velocity and the seabed perturbation in the x direction.
ϕ_v	Spatial phase lag between the velocity and the seabed perturbation in the y direction.
g	Gravity acceleration [m s^{-2}].
h	Bed form amplitude [m].
H	Water depth [m].
k	Wave number component in the x direction [m^{-1}].
l	Wave number component in the y direction [m^{-1}].
λ	Bed slope coefficient.
l_m	Tidal excursion length [m].
ω_g	Dimensionless growth rate.
p	Bed porosity [dimensionless].
q_b	Bed load sediment flux [kg m^{-1} s^{-1}].

q_s Suspended load sediment flux [kg m^{-1} s^{-1}].
u Current velocity [m s^{-1}].
u_c Critical velocity [m s^{-1}].
$\hat{r}$ Dimensionless friction coefficient.
ρ Water density [kg m^{-3}].
ρ_s Sediment density [kg m^{-3}].
σ Tidal frequency [s^{-1}].
$\vec{S}_b$ Sediment flux [kg m^{-1} s^{-1}].
T_m Morphological time scale [s].
T_{m2} Morphological doubling time [s].
τ_c Critical bed shear stress [kg m^{-1} s^{-2}].
ξ Free surface level [m].
z_b Bed level [m].

[57] **Acknowledgments.** The authors thank P. Roos for all the fruitful discussions, P. Le Hir, whose remarks are at the origin of this investigation on grain size dependency, and the three reviewers of the present paper for their remarks and suggestions. This work has been financially supported by the EUMARSAND European project and internal research funds of BRGM.

References

Balson, P. S., C. Laban, R. T. E. Schttenhelm, R. Paepe, and C. Baeteman (1991), Ostend: Sheet 52N/02E, in *British Geological Survey 1:250000 Series: Sea Bed Sediments and Holocene Geology*, Br. Geol. Surv., Nottingham, U. K.

Besio, G., P. Blondeaux, and G. Vittori (2006), On the formation of sand waves and sand banks, *J. Fluid Mech.*, *557*, 1–27.

Cameron, T. D. J., C. Laban, and R. T. E. Schttenhelm (1984), Flemish Bight: Sheet 52N/02E, in *British Geological Survey 1:250000 Series: Sea Bed Sediments and Holocene Geology*, Br. Geol. Surv., Nottingham, U. K.

Collins, M. B., S. J. Shimwell, S. Gao, H. Powell, C. Hewistom, and J. A. Taylor (1995), Water and sediment movement in the vicinity of linear sandbanks: The Norfolk Banks, southern North Sea, *Mar. Geol.*, *123*, 125–142.

de Swart, H., and S. J. M. H. Hulscher (1995), Dynamics of large-scale bed forms in coastal seas, in *Nonlinear Dynamics and Pattern Formation in the Natural Environment*, edited by A. Doelamn and A. van Harten, pp. 315–331, Longman, Essex, U. K.

Engelund, F., and E. Hansen (1967), *A Monograph on Sediment Transport in Alluvial Streams*, Tknisk Forlag, Copenhagen.

Fluit, C. C., and S. J. M. H. Hulscher (2002), Morphological response to a North Sea bed depression induced by gas mining, *J. Geophys. Res.*, *107*(C3), 3022, doi:10.1029/2001JC000851.

Harrison, D. J., C. Laban, and R. T. E. Schttenhelm (1987), Indefatigable: Sheet 53N/02E, in *British Geological Survey 1:250000 Series: Sea Bed Sediments and Holocene Geology*, Br. Geol. Surv., Nottingham, U. K.

Hulscher, S. J. M. H., H. E. De Swart, and H. J. De Vriend (1993), The generation of offshore tidal sand banks and sand waves, *Cont. Shelf Res.*, *13*, 1183–1204.

Huthnance, J. M. (1982), On one mechanism forming linear sand banks, *Estuarine Coastal Shelf Sci.*, *14*, 79–99.

Idier, D. (2002), Dynamique des bancs et dunes de sable du plateau continental, observations in-situ et modlisation numrique, Ph.D. thesis, Inst. Natl. Polytech. de Toulouse, Toulouse, France.

Idier, D., and D. Astruc (2003), Analytical and numerical modeling of large-scale rhythmic bedform dynamics, *J. Geophys. Res.*, *108*(C3), 3060, doi:10.1029/2001JC001205.

Knaapen, M. A. F. (2008), Sandbank occurrence on the Dutch continental shelf in the North Sea, *Geo Mar. Lett.*, *29*, 17–24, doi:10.1007/s00367-008-0105-7.

Meyer-Peter, A., and R. Muller (1948), Formulas for bedload transport, paper presented at second congress, IAHR, Stokholm, Sweden.

Off, T. (1963), Rhythmic linear sand bodies caused by tidal currents, *Am. Assoc. Pet. Geol. Bull.*, *47*, 324–341.

Rijks Geologische Dienst (1984), Geological charts of the North Sea: Indefatigable, Flemish Bight, Ostend., Haarlem, Netherlands.

Roos, P. C. (2004), Seabed pattern dynamics and offshore sand extraction, Ph.D. thesis, Univ. of Twente, Enschede, Netherlands.

Roos, P. C., R. Wemmenhove, S. J. M. H. Hulscher, H. W. M. Hoeijmakers, and N. P. Kruyt (2007), Modeling the effect of nonuniform sediment on the dynamics of offshore tidal sandbanks, *J. Geophys. Res.*, *112*, F02011, doi:10.1029/2005JF000376.

Smith, W. H. F., and D. T. Sandwell (1997), Global seafloor topography from satellite altimetry and ship depth soundings, *Science*, *217*, 1957–1962.

Stride, A. H. (1982), *Offshore Tidal Sands*, Chapman and Hall, London.

Trentesaux, A., A. Stolk, B. Tessier, and H. Chamley (1994), Surficial sedimentology of the Middlekerke Bank (southern North Sea), *Mar. Geol.*, *121*, 43–55.

Van den Brink, G. M. (1998), Prediction of sand wave occurrence, M.S. thesis, Water Eng. and Manage, Univ. of Twente, Enschede, Netherlands.

Van der Veen, H. H. (2008), Natural and human induced seabed evolution: The occurrence of large scale bed patterns and the effects of human activities on the North Sea seabed, Ph.D. thesis, Univ. of Twente, Twente, Netherlands.

Van der Veen, H. H., S. J. M. H. Hulscher, and M. A. F. Knaapen (2005), Grain size dependency in the occurrence of sand waves, *Ocean Dyn.*, *56*, 228–234, doi:10.1007/s10236-005-0049-7.

van Lancker, V. (1999), Sediment and morphodynamics of a silicoclastic near coastal area, in relation to hydrodynamical and meteorological conditions: Belgian continental shelf, Ph.D. thesis, Univ. of Gent, Gent, Belgium.

van Rijn, L. C. (1984), Sediment transport, Part I: Bedload transport, *J. Hydraul. Eng.*, *110*(10), 1431–1456.

van Rijn, L. C. (1989), Handbook: Sediment transport by currents and waves, *Rep. H 461*, Delft Hydraul., Delft, Netherlands.

Verlaan, M., A. Zijderveld, H. De Vries, and J. Kroos (2005), Operational storm surge forecasting in the Netherlands: Developments in the last decade, *Philos. Trans. R. Soc., Ser. A*, *363*, 1441–1453, doi:10.1098/rsta.2005.1578.

Walgreen, M., D. Calvete, and H. de Swart (2002), Growth of large-scale bedforms due to storm-driven and tidal currents: A model approach, *Cont. Shelf Res.*, *22*, 2777–2793.

Walgreen, M., H. de Swart, and D. Calvete (2004), A model for grain-size sorting over tidal sand ridges, *Ocean Dyn.*, *54*, 374–384, doi:10.1007/s10236-004-0066-3.

Wentworth, C. K. (1922), A scale of grade and class terms for clastic sediments, *J. Geol.*, *30*, 377–392.

S. J. M. H. Hulscher and H. H. van der Veen, Water Engineering and Management, University of Twente, P.O. Box 217, NL-7500 AE Enschede, Netherlands. (H.H.vanderVeen@ctw.utwente.nl; S.J.M.H.Hulscher@ctw.utwente.nl)

D. Idier, BRGM, 3 Avenue C. Guillemin, BP 6009, F-45060 Orléans CEDEX 2, France. (d.idier@brgm.fr)